Electronic Communication in Oligometallic Complexes with Ferrocene-Based Tris(1-pyrazolyl)borate Ligands

ShengLi Guo,[†] Frank Peters,[‡] Fabrizia Fabrizi de Biani,[§] Jan W. Bats,[#] Eberhardt Herdtweck,[£] Piero Zanello,[§] and Matthias Wagner*[,†]

Institut für Anorganische Chemie and Institut für Organische Chemie, J. W. Goethe-Universität Frankfurt, Marie-Curie-Str. 11, D-60439 Frankfurt (Main), Germany, Bayer AG, D-51368 Leverkusen, Germany, Dipartimento di Chimica dell′Università, Via Aldo Moro, I-53100 Siena, Italy, and Institut für Anorganische Chemie der Technischen Universität München, Lichtenbergstr. 4, D-85747 Garching, Germany

Received October 31, 2000

Ferrocene-based tris(1-pyrazolyl)borate ligands **1R**−**Li** and **1R**−**Tl** have been synthesized and used to generate a variety of heterotrinuclear transition metal complexes, **3R**−**M** [R = H, $SiMe_3$, cyclohexyl, (cyclohexyl)methyl, phenyl; M(II) = Mn, Fe, Co, Ni, Cu, Zn]. The poor solubility of **3H**−**M** is greatly enhanced by the introduction of large organic substituents into the 4-positions of all pyrazolyl rings. The unsubstituted ligand **1H**−**Li** and the trinuclear complex **3Cym**−**Cu** [Cym = (cyclohexyl)methyl] have been investigated by X-ray crystallography. **1H**−**Li**, which represents the first example of a structurally characterized lithium tris(1-pyrazolyl)borate, forms centrosymmetric dimers in the solid state. A severe Jahn−Teller distortion was observed for the $(Bpz_3)_2Cu$ fragment in **3Cym**−**Cu**. Compared to the parent compounds [$(HBpz_3)_2M$], the presence of uncharged ferrocenyl substituents in **3R**−**M** tends to shift the M^{2+}/M^{3+} redox potential to significantly more cathodic values. The opposite is true if the ferrocenyl fragments are in their cationic state, which results in an anodic shift of the M^{2+}/M^{3+} transition. Most interestingly, the two ferrocenyl fragments in **3R**−**Cu** appear to be electronically communicating.

Introduction

In the ongoing search for novel magnetic and (semi)-conducting materials, metal-containing polymers are receiving increasing attention.[1] Ferrocene is a particularly well-suited building block for the generation of macromolecules, since it is easy to derivatize, shows a reversible one-electron oxidation (leading to a paramagnetic state), and provides a relatively rigid molecular framework. However, despite of numerous efforts, no tractable high molecular weight polymers with ferrocene in the backbone had been available until 1992, when Manners invented the synthesis of poly(ferrocenylene)s via the ring-opening polymerization of strained, ring-tilted *ansa*-ferrocenophanes.[2,3]

Our group investigates alternative ways to organometallic polymers, trying to combine the advantages of coordination polymer synthesis with the electronic properties of ferrocene-containing materials. One promising approach employs ferrocene-based tris(1-pyrazolyl)borate ("scorpionate")[4] ligands **1H**−**M** and **2H**−**Li** (Figure 1). Upon reaction with divalent transition metals M(II), these molecules can be expected to offer convenient access to heterotrinuclear complexes (**3H**−**M**, Scheme 1) and to polymeric materials $[1,1'\text{-fc}(Bpz_3)_2M]_n$ (fc = $(C_5H_4)_2Fe$; pz = 1-pyrazolyl).

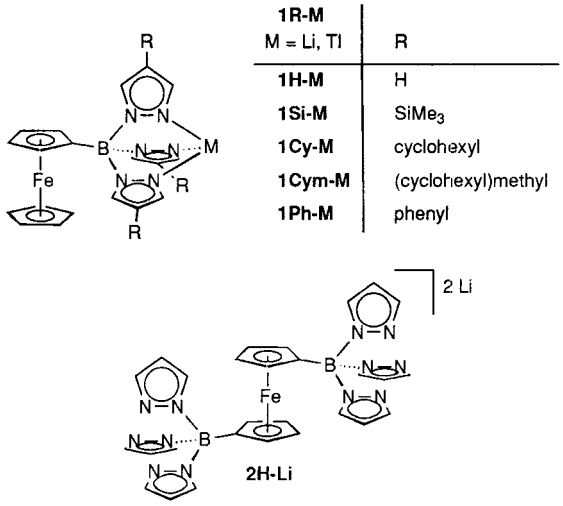

Figure 1. Mono- and difunctional ferrocene-based tris(1-pyrazolyl)-borate ligands.

High-yield syntheses of **1R**−**M** (R = H, $SiMe_3$; M = Li, Tl) and **2H**−**Li** have already been reported by our group. Various transition metal complexes of these ligands have been characterized and studied by cyclic voltammetry.[5−7]

* To whom communication should be addressed. Telefax: +49-69-798-29260. E-mail: Matthias.Wagner@chemie.uni-frankfurt.de.
[†] Institut für Anorganische Chemie, J. W. Goethe-Universität Frankfurt.
[‡] Bayer AG.
[§] Dipartimento di Chimica dell′Università.
[#] Institut für Organische Chemie, J. W. Goethe-Universität Frankfurt.
[£] Institut für Anorganische Chemie der Technischen Universität München.

(1) *Metal-Containing Polymeric Materials*; Pittman, C. U., Carraher, C. E., Zeldin, M., Sheats, J. E., Culbertson, B. M., Eds.; Plenum Press: New York, 1996.
(2) Foucher, D. A.; Tang, B.-Z.; Manners, I. *J. Am. Chem. Soc.* **1992**, *114*, 6246−6248.
(3) Manners, I. *Adv. Organomet. Chem.* **1995**, *37*, 131−168.
(4) Trofimenko, S. *Scorpionates*; Imperial College Press: London, 1999.
(5) Jäkle, F.; Polborn, K.; Wagner, M. *Chem. Ber.* **1996**, *129*, 603−606.
(6) Fabrizi de Biani, F.; Jäkle, F.; Spiegler, M.; Wagner, M.; Zanello, P. *Inorg. Chem.* **1997**, *36*, 2103−2111.

10.1021/ic001199j CCC: $20.00
Published on Web 08/14/2001

Scheme 1. Syntheses of **3R−M**[a]

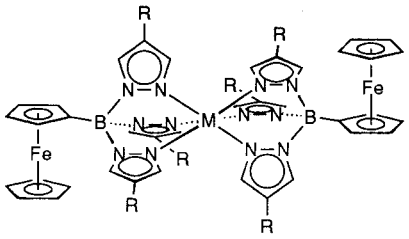

M(II)	R = H	$SiMe_3$	cyclohexyl	(cyclohexyl) methyl	phenyl
Mn	**3H-Mn**	--	--	--	--
Fe	**3H-Fe**	**3Si-Fe**	--	--	--
Co	**3H-Co**	--	--	--	--
Ni	**3H-Ni**	--	--	--	--
Cu	**3H-Cu**	**3Si-Cu**	**3Cy-Cu**	**3Cym-Cu**	**3Ph-Cu**
Zn	**3H-Zn**	--	--	--	--

Syntheses:

1H-Li + MCl_2 —(i)→ **3H-M**

1H-Tl + $NiBr_2 \cdot 2\,THF$ —(ii)→ **3H-Ni**

1R-Tl + $CuBr_2$ —(iii)→ **3R-Cu**

[a] (i) THF/Water, r.t.; (ii) THF, r.t.; (iii) Toluene, r.t., R = $SiMe_3$, cyclohexyl, (cyclohexyl)methyl, and phenyl.

The purpose of this paper is to describe heterotrinuclear complexes **3H−M** (M(II) = Mn, Fe, Co, Ni, Cu, Zn) and to answer the question as to whether there is electronic communication between the individual metal centers. Moreover, novel derivatives **1R−M** [R = cyclohexyl, (cyclohexyl)methyl, phenyl; M = Li, Tl; Figure 1] of the ligand system are described, which give transition metal complexes **3R−M** (Scheme 1) of greatly enhanced solubility.

Results and Discussion

Syntheses. We generally employed the lithium salts **1H−Li** for the syntheses of complexes **3H−M**. **3H−M** (M(II) = Mn, Fe,[5] Co, Ni, Cu, Zn) are readily obtained as microcrystalline precipitates upon addition of the respective metal chlorides in water to a solution of **1H−Li** in THF. The Fe(II) complex **3H−Fe** is slowly oxidized when exposed to air. As a result, its NMR spectra often suffered from line broadening due to paramagnetic impurities, even though carefully degassed water was used. It is therefore advantageous to synthesize **3H−Fe** in a heterogeneous reaction by mixing $FeCl_2$ and **1H−Li** in THF, which has been freshly distilled from potassium/benzophenone. **3H−Ni** was also obtained under anhydrous conditions from **1H−Tl** and $NiBr_2 \cdot 2THF$ in THF.

In an attempt to generate a cationic Cr(III) complex bearing two ferrocenylscorpionate ligands, a solution of **1H−Li** in THF/H_2O was treated dropwise at room temperature with $CrCl_3 \cdot 6H_2O$. However, this reaction resulted in the complete breakdown of the scorpionate moiety with almost quantitative formation of triferrocenylboroxine **4** (Figure 2).

4 was also isolated from mixtures of the sterically congested ligand $FcB(pz^{3-Ph})_3Li$ and $ZnCl_2$ in THF/H_2O (Fc = ferrocenyl; pz^{3-Ph} = 3-phenylpyrazolyl).[8] The fact, that **1H−Li** is readily hydrolyzed with clean formation of **4** is somewhat surprising, since previous attempts to synthesize this compound either from $FcBBr_2$ and $Me_3Si-O-SiMe_3$ or by careful hydrolysis of $FcBX_2$ (X = Br, NMe_2) have only been of limited success.[9]

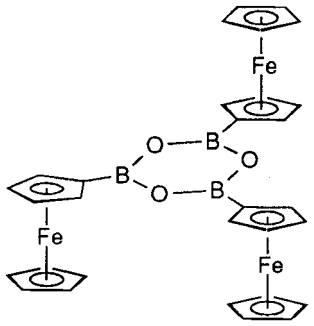

4

Figure 2. Triferrocenylboroxine formed by hydrolysis of **1H−Li** in the presence of $CrCl_3$.

All compounds **3H−M** possess a very low solubility in hexane and benzene, but, except for the copper complex, are moderately soluble in CH_2Cl_2 and $CHCl_3$. **3H−Cu** suffers from poor solubility in all common solvents. Since cyclic voltammetry measurements revealed very special redox properties of this compound (see below), it was of crucial importance to exclude contamination of the sample with electrochemically active byproducts and to get derivatives of higher solubility, which allow purification by chromatography or recrystallization. Thus, solubilizing substituents R were introduced into the 4-position of the pyrazole rings (R = $SiMe_3$,[10] cyclohexyl,[11] (cyclohexyl)-methyl,[11] phenyl[11]). Ligand syntheses (**1Si−Tl**, **1Cy−Tl**, **1Cym−Tl**, **1Ph−Li**; Figure 1) were achieved by the established procedure,[5] and the corresponding copper complexes **3Si−Cu**, **3Cy−Cu**, **3Cym−Cu**, and **3Ph−Cu** were obtained in decent yield upon reaction of the respective thallium or lithium scorpionates with $CuBr_2$. Especially the first three compounds are highly soluble in toluene and can readily be purified by column chromatography.

Spectroscopy. UV−vis spectra of complexes **3H−M** (M(II) = Co, Ni, Cu, Zn) in CH_2Cl_2 exhibit a strong absorption at λ = 235 nm, with a shoulder at λ = 332 nm. In addition, a very broad band appears at higher wavelengths (λ_{max} [nm] = 460, Co; 458, Ni; 440, Cu; 450, Zn). The electronic absorption spectra of all four compounds are thus rather similar and dominated by the absorptions of the ferrocenyl fragments. This interpretation is confirmed by the observation that a purple solution of $[HB(pz^{3,5-Me})_3]_2Ni$ ($pz^{3,5-Me}$ = 3,5-dimethylpyrazolyl) adopts a yellow color upon addition of 2 equiv of ferrocene.

The infrared spectra (KBr) of **3H−M** (M(II) = Mn, Fe, Co, Ni, Cu, Zn) are almost identical and very similar to the IR spectrum of the lithium scorpionate **1H−Li**. According to Rheingold et al.,[12] this finding suggests that all seven tris(1-pyrazolyl)borate complexes possess closely related molecular structures in the solid state. This assumption is supported by the results of X-ray crystal structure analyses of **1H−Li** and **3Cym−Cu** (see below).

All NMR spectra of the ligands **1Si−Tl**, **1Cy−Tl**, **1Cym−Tl**, and **1Ph−Li** show the expected[5] signal patterns and thus

(7) Herdtweck, E.; Peters, F.; Scherer, W.; Wagner, M. *Polyhedron* **1998**, *17*, 1149−1157.
(8) Peters, F. Ph.D. Thesis, Technische Universität München, 1998.
(9) Nöth, H., personal communication.
(10) Birkofer, L.; Franz, M. *Chem. Ber.* **1972**, *105*, 1759−1767.
(11) Tolf, J.-R.; Piechaczek, J.; Dahlbom, R.; Theorell, H.; Åkeson, Å.; Lundquist, G. *Acta Chem. Scand.* **1979**, *B33*, 483−487.
(12) Rheingold, A. L.; Yap, G. P. A.; Liable-Sands, L. M.; Guzei, I. A.; Trofimenko, S. *Inorg. Chem.* **1997**, *36*, 6261−6265.

do not merit further discussion. The NMR spectra of their corresponding transition metal complexes are more complicated, and one has to distinguish between the diamagnetic complexes **3H−Fe** and **3H−Zn**, on one hand, and the paramagnetic species **3H−Mn**, **3H−Co**, **3H−Ni**, and **3R−Cu**, on the other.

The ^{11}B NMR spectra of **3H−Fe** and **3H−Zn** exhibit one sharp signal in the chemical shift range of tetracoordinated boron nuclei[13] (**3H−Fe**: $\delta = -1.0$;[5] **3H−Zn**: $\delta = -0.6$). In the ^{1}H NMR spectra, one set of signals is observed for both ferrocenylscorpionate ligands, and all pyrazolyl rings are magnetically equivalent. The same holds for the ^{13}C NMR spectra. **3H−Fe** and **3H−Zn** thus possess highly symmetric structures with six-coordinate metal centers. At room temperature, the pyrazolyl protons of both complexes give broad, poorly resolved NMR signals, which sharpen up considerably when the spectra are run at elevated temperatures. The resonance of H5, the pyrazolyl proton closest to the ferrocenyl substituent, shows the most pronounced temperature effect, which is therefore likely due to a hindered rotation about the B−Cp bond.[6] Unfavorable steric interactions between the ferrocenyl moiety and the tris(1-pyrazolyl)borate fragment[7] are not only responsible for this high rotational barrier, but also prevent the synthesis of ferrocene-based scorpionates with substituents bulkier than hydrogen in the 5-position of the pyrazolyl rings (e.g., 3, 5-dimethylpyrazolyl).

^{1}H and ^{11}B NMR spectra of the paramagnetic complexes with M(II) = Mn, Co, Ni, Cu were recorded at 303 K in $CDCl_3$ on a 400 MHz spectrometer. Resonances were assigned by comparison with the NMR spectra of the ferrocene-free compounds [$(HBpz_3)_2$M], which have been thoroughly studied by Feher and Köhler, at temperatures ranging from 298 to 305 K.[14] In most cases, the proton chemical shift values were in reasonably good agreement. However, the above-mentioned line broadening due to hindered molecular motion led to substantial differences in the half-widths of related resonances of **3H−M** and [$(HBpz_3)_2$M]. Nevertheless, we chose not to run the ^{1}H NMR spectra at elevated temperatures, since paramagnetic shift values are strongly dependent on temperature, and we wanted to ensure maximum comparability of these data with the results obtained in the Köhler group.

In the case of **3H−Mn**, only two signals at $\delta^{exp} = 1.4$ ($h_{1/2} = 80$ Hz) and $\delta^{exp} = 4.5$ ($h_{1/2} = 330$ Hz) were detectable in the ^{1}H NMR spectrum (note: in the following discussion, the term δ^{exp} is used for the experimentally determined chemical shift values at 303 K). The resonances of the pyrazolyl protons in [$(HBpz_3)_2$Mn] possess half-widths between 3700 Hz (H5) and 10800 Hz (H4).[14] Since complexes **3H−M** usually show much broader pyrazolyl signals compared to the ferrocene-free species, we tentatively assign the two resonances of **3H−Mn** to its ferrocenyl protons. Similar arguments hold for **3H−Cu**. Again, only two proton signals, most likely those of the ferrocenyl substituents, are observed [$\delta^{exp} = 1.5$ ($h_{1/2} = 25$ Hz) and $\delta^{exp} = 4.4$ ($h_{1/2} = 50$ Hz)]. NMR spectroscopy is thus of little diagnostic value in the case of **3H−Mn** and **3H−Cu**. The copper complexes **3Si−Cu**, **3Cy−Cu**, **3Cym−Cu**, and **3Ph−Cu** each give additional signals, which are attributable to the individual pyrazolyl substituents. An inspection of the respective integrals shows all four complexes to possess a pyrazolyl: ferrocenyl ratio of 3:1, which is in agreement with the proposed molecular structures.

More structural information can be gained from the NMR spectra of **3H−Co** and **3H−Ni**, since they show much sharper resonances and thus have considerably improved signal-to-noise ratios. The ^{11}B NMR spectrum of **3H−Co** exhibits one resonance at 240 ppm, which is close to the value found for its mononuclear counterpart [$(HBpz_3)_2$Co] ($\delta^{exp} = 262$). In the ^{1}H NMR spectrum, six signals corresponding to the six sets of magnetically nonequivalent protons can be identified. Of those, two resonances at −121 and 96 ppm are likely to belong to the pz-H3 and pz-H5, respectively.[14] The other four signals possess similar chemical shifts of $\delta^{exp} = 22$, 25, 35, and 51, and have to be assigned to pz-H4 and the ferrocenyl moieties. Any further interpretation would have to remain highly speculative, since the pz-H4 protons of [$(HBpz_3)_2$Co] were found at 40 ppm, which is very close to at least two of the four signals under discussion in **3H−Co**. In the case of the nickel complex **3H−Ni**, the NMR spectra ($\delta^{exp}(^{11}B) = -38$; $\delta^{exp}(^{1}H) = 4.3$, 4.5 [$C_5H_5$, C_5H_4], 40 [pz-H3], 46.6, 54.2 [pz-H4,5]) are in good agreement with the data published for [$(HBpz_3)_2$Ni].[14]

Important parameters for further discussion are the paramagnetic shifts δ^{para}. They can be calculated from the experimentally obtained values δ^{exp} and the chemical shifts δ^{dia} of analogous nuclei in a closely related diamagnetic compound, using the formula $\delta^{para} = \delta^{exp} - \delta^{dia}$. We have employed the iron complex **3H−Fe** as a diamagnetic reference system.[5] The protons of the ferrocenyl substituents show negligible paramagnetic shifts in the case of **3H−Ni** ($\delta^{para} < 0.4$), but are influenced considerably by the cobalt center in **3H−Co** ($17.4 < \delta^{para} < 47$; note: a more precise value of δ^{para} cannot be given due to uncertainties in the assignments of the corresponding δ^{exp} values). In both complexes, the paramagnetic shifts are much more pronounced for the pyrazolyl protons compared to the cyclopentadienyl protons (**3H−Ni**: $\delta^{para} = 33$ [pz-H3]; $39 < \delta^{para} < 48$ [pz-H4,5]; **3H−Co**: $\delta^{para} = -128$ [pz-H3], 89 [pz-H5]).

Two important terms contribute to δ^{para}, which are (i) Fermi contact coupling and (ii) dipolar coupling. The Fermi contact shift is an isotropic through-bond effect. In contrast, dipolar coupling is transmitted through space and thus depends on geometric factors. In the case of octahedrally coordinated Co(II) scorpionates, both Fermi contact coupling and dipolar coupling have to be considered, while δ^{para} values of octahedral Ni(II) complexes are dominated by the Fermi contact term. One possible interpretation of the small δ^{para} values of the cyclopentadienyl protons in **3H−Ni** would be that only a little spin density is delocalized from the paramagnetic Ni center onto the ferrocenyl substituents. It has, however, to be taken into account that Fermi contact and dipolar coupling can have opposite signs.

The mass spectra (CI and ESI mode) of all complexes **3H−M** exhibit peaks of high intensity, attributable to the cations [**3H−M**]$^{+}$. No major fragmentation is observed in the gas phase except in the case of **3H−Cu**, which formally loses $Cu(pz)_2$ to form a dinuclear ferrocene compound with pyrazabole[15] bridge, [FcB(pz)(μ-pz)]$_2$ (660 amu; 55%)].

Electrochemical Properties of 3H−M and 3R−Cu (R = Si, Cy, Cym, Ph). Figure 3, which compares the cyclic voltammetric response of **3H−Ni** with that of **3H−Cu** in dichloromethane solution, gives an overall picture of the different redox behavior of complexes **3R−M** (M = Mn, Fe, Co, Ni, Zn) with respect to **3R−Cu**.

3H−Ni undergoes a first oxidation ($E^{\circ\prime} = +0.45$ V) possessing features of chemical reversibility, followed by a further chemically reversible anodic process ($E^{\circ\prime} = +1.29$ V).

(13) Nöth, H.; Wrackmeyer, B. *Nuclear Magnetic Resonance Spectroscopy of Boron Compounds*; Springer-Verlag: Berlin, Heidelberg, New York, 1978.

(14) Feher, R. Ph.D. Thesis, Technische Universität München, 1996.

(15) Trofimenko, S. *J. Am. Chem. Soc.* **1967**, *89*, 3165−3170.

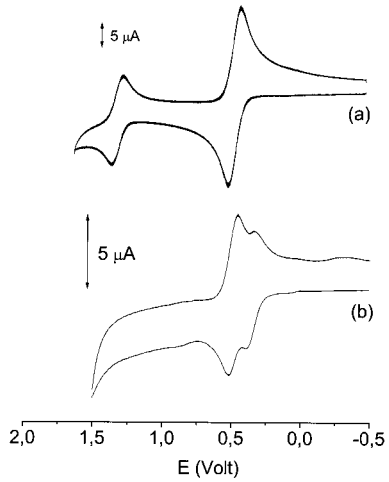

Figure 3. Cyclic voltammetric responses recorded at a platinum electrode on CH_2Cl_2 solutions containing $[NBu_4][PF_6]$ and (a) **3H**−**Ni** (0.9×10^{-3} mol dm^{-3}), (b) **3H**−**Cu** (saturated solution). Scan rate 0.2 Vs^{-1}

The height of the peak corresponding to the second process is about one-half of that of the first one. Considering the nature of the molecule, we may safely assume that the first step involves the concomitant one-electron oxidation of the two peripheral ferrocenyl subunits, whereas the most anodic step involves the one-electron oxidation of the central Ni(II)−scorpionate core. In fact, controlled potential electrolysis corresponding with the first oxidation ($E_w = +0.8$ V) consumes two electrons per molecule. As a consequence of the exhaustive oxidation, the initially pale yellow solution turns light blue (λ_{max} = 630 nm; typical value for ferricenium species). It exhibits cyclic voltammetric profiles that are quite complementary to the original ones, which confirms the chemical reversibility of the two-electron process. Analysis of the cyclic voltammograms relative to the two-electron oxidation with scan rates varying from 0.02 to 1 Vs^{-1} shows that (a) the current ratio i_{pc}/i_{pa} is constantly equal to one, (b) the current function $i_{pa}/v^{1/2}$ remains constant, and (c) the peak-to-peak separation ΔE_p increases from 76 mV at 0.02 Vs^{-1} to 151 mV at 1.0 Vs^{-1}. The fact that the ΔE_p values are always greater than 60 mV suggests that the two one-electron oxidations occur at the same standard electrode potentials. A similar cyclic voltammetric analysis diagnostic for a simple one-electron process holds for the second, Ni-centered, oxidation. As Table 1 compiles, a qualitatively similar voltammetric picture indicative of a single two-electron oxidation of the ferrocenyl groups is exhibited by the other complexes **3R**−**M** (M = Mn, Fe, Co, Zn).

Some differences hold as far as the electrochemical behavior of the central metal cores is concerned. In **3H**−**Zn**, obviously no oxidation occurs, whereas in the cases of **3H**−**Mn**, **3R**−**Fe**, and **3H**−**Co**, the M^{2+}/M^{3+} oxidation precedes the ferrocenyl oxidations. For **3H**−**Mn**, the Mn^{2+}/Mn^{3+} transition is irreversible. In **3H**−**Ni**, nickel oxidation follows the ferrocenyl oxidations. It is interesting to note that the nickel center of **3H**−**Ni** is somewhat harder to oxidize than that of $[(HBpz_3)_2Ni]$ ($\Delta E^{\circ\prime}$ = 0.17 V; Table 1). We attribute this to the higher coulombic repulsion experienced by the $[\mathbf{3H}-\mathbf{Ni}]^{2+/3+}$ redox change with respect to the corresponding $[(HBpz_3)_2Ni]^{0/+}$ oxidation. In contrast, the M^{2+}/M^{3+} transition in **3R**−**Fe** and **3H**−**Co** shows significant shifts of $\Delta E^{\circ\prime}$ to lower potential values compared with the corresponding ferrocene-free species $[(HBpz_3)_2M]$ (e.g., **3H**−**Fe**, $\Delta E^{\circ\prime} = 0.28$ V; **3H**−**Co**, $\Delta E^{\circ\prime} = 0.34$ V; Table 1).

As in the case of **3H**−**Ni**, the exhaustive two-electron oxidation of **3H**−**Zn** causes the initially pale yellow solution to turn light blue (λ_{max} = 630 nm). Based on controlled potential coulometric experiments, the **3H**−**Fe**, **3Si**−**Fe**, and **3H**−**Co** complexes have been found to be stable both in the monocationic and tricationic states. The pale yellow solution of **3H**−**Co** turns bright yellow after the Co^{2+}/Co^{3+} oxidation and green-blue (λ_{max} = 630 nm) after the oxidation of the ferrocene moieties. The broad EPR signal of the neutral compound, which is isotropic and not finely resolved ($g = 2.36$), disappears after the first oxidation, thereby confirming the assignment of this process to the Co^{2+}/Co^{3+} redox change. An interesting behavior has been observed for the **3Si**−**Fe** complex; upon oxidation of the neutral molecule to its monocationic form, the initially pale orange solution turns to very intense ruby red. A broad UV−vis band appears, encompassing the region from 350 to 600 nm. Further exhaustive two-electron oxidation causes the solution to become brown, and a shoulder at 630 nm is added to the UV−vis spectrum.

Table 1. Formal Electrode Potentials (in V versus SCE), Peak-to-Peak Separations (in mV), Redox Potential Differences (in mV), and Comproportionation Constants for the Redox Processes of the **3R**−**M** Scorpionate Complexes in CH_2Cl_2 Solution (with 0.2 M $[NBu_4][PF_6]$ as Electrolyte)

	Fc-centered process				M-centered processes	
	$E^{\circ\prime}$	ΔE_p[a]	$\Delta E^{\circ\prime}$[b]	K_{com}	$E^{\circ\prime}$	ΔE_p[a]
3H−**Mn**	+0.54[c]	74	−	−	+0.37[d]	−
3H−**Fe**	+0.54[c]	72	−	−	+0.04	64
3Si−**Fe**	+0.57[c]	76	−	−	+0.06	74
3H−**Co**	+0.53[c]	78	−	−	−0.36	243
3H−**Ni**	+0.45[c]	80	−	−	+1.29	76
3H−**Zn**	+0.45[c]	78	−	−	−	−
3H−**Cu**	+0.36/+0.49	86/74	130	160	−1.4[e]	−
3Si−**Cu**	+0.40/+0.53	80/100	130	160	−1.6[e]	−
3Cy−**Cu**	+0.39/+0.54	74/53	150	340	−1.7[e]	−
3Cym−**Cu**	+0.33/+0.50	66/66	170	750	−1.7[e]	−
3Ph−**Cu**	+0.46/+0.58	60/73	120	100	−1.7[e]	−
Tp$_2$Fe[f]	−	−	−	−	+0.32	rev
Tp$_2$Co[g]	−	−	−	−	−0.02	quasirev
Tp$_2$Ni[g]	−	−	−	−	+1.12	irrev
FcH	+0.39	89	−	−	−	−

[a] Measured at 0.2 V/s. [b] Difference of the redox potentials of the two ferrocene oxidations in **3R**−**Cu**. [c] Two-electron process. [d] Peak potential for the irreversible Mn^{2+}/Mn^{3+} transition. [e] Peak potential for the irreversible Cu^{+}/Cu^{2+} transition. [f] Tp: hydridotris(1-pyrazolyl)borate; lit.[29] [g] Lit.[14]

The electrochemical behavior of the **3R**−**Cu** complexes (R = H, Si, Cy, Cym, Ph) shows striking differences to that of all other compounds **3R**−**M**. As exemplified in Figure 3, all derivatives **3R**−**Cu** exhibit two well-resolved oxidation waves. This must be attributed to the sequential one-electron oxidation of the two ferrocene groups, taking into account that the reversible access to the Cu^{2+}/Cu^{3+} oxidation is allowed only for strictly planar geometries (in confirmation, $[(HBpz_3)_2Cu]$ undergoes an irreversible oxidation at $E_p = +2.91$ V versus SCE).[14] This preliminarily means that the two iron centers are electronically communicating. Given the rigid molecular framework of the ferrocenylscorpionate ligands, all molecules **3R**−**M** are expected to possess rather similar Fc···M− and Fc···Fc distances. The very peculiar electrochemical behavior of **3R**−**Cu** is not observed for any of the other complexes and, thus, cannot be attributed to simple coulombic repulsion between the two positively charged ferrocenyl centers. Moreover, X-ray crystallography shows both halves of **3Cym**−**Cu** to be chemically equivalent (see below). Since the molecule can be assumed to possess a similar symmetry in solution, no differences in the coordination behavior of the scorpionate ligands are likely to be responsible for the appearance of two separate oxidation steps. It is therefore tempting to ascribe this effect to an

Table 2. Summary of Crystallographic Data of $(\mathbf{1H-Li})_2 \cdot 4C_6H_6$ and $\mathbf{3Cym-Cu} \cdot 2C_7H_8$

	$(\mathbf{1H-Li})_2 \cdot 4C_6H_6$	$\mathbf{3Cym-Cu} \cdot 2C_7H_8$
chem formula	$C_{38}H_{36}B_2Fe_2Li_2N_{12}$ $4C_6H_6$	$C_{80}H_{108}B_2CuFe_2N_{12}$ $2C_7H_8$
fw	1120.42	1618.91
space group	$P-1$(No. 2)	$P-1$(No. 2)
a/Å	9.8951(5)	10.541(4)
b/Å	11.5287(6)	13.099(5)
c/Å	13.6197(7)	16.609(7)
α/deg	111.168(5)	96.530(9)
β/deg	99.008(5)	101.598(11)
γ/deg	100.404(5)	102.849(9)
V/Å^3	1382.8(1)	2159.7(15)
Z	1	1
T /K	193(1)	136(2)
λ /Å	0.71073	0.71073
ρ_{calcd}/g cm^{-3}	1.345	1.245
μ/mm^{-1}	0.577	0.628
$R1^a$ ($I_o > 2\sigma(I_o)$/all data)	0.0275/0.0399	0.1482/0.2695
$wR2^b$(all data)	0.0643	0.2880

^{a} $R1 = \sum(||F_o| - |F_c||)/\sum|F_o|$. ^{b} $wR2 = [\sum w(F_o^2 - F_c^2)^2/\sum w(F_o^2)^2]^{1/2}$.

electronic interaction of the two ferrocenyl centers in **3R−Cu**. Nevertheless, the through-space or through-bond origin of this phenomenon surely deserves further investigation. The separation $\Delta E^{\circ\prime}$ (in V) of the two redox potentials in **3R−Cu** allows us to estimate the stability of the mixed-valent monocations [Fe(II)−Cu(II)−Fe(III)]$^+$ by calculating the respective values of the comproportionation constant K_{com} (at 25 °C; for two consecutive one-electron steps it holds that $K_{com} = 10^{\{16.9\Delta E^{\circ\prime}\}}$; $\Delta E^{\circ\prime}$ in [V]). Depending on the substituents R, the values roughly range from 100 to 800, indicating the presence of slightly delocalized mixed-valent species (Table 1).

The **3R−Cu** complexes have been exhaustively oxidized in two steps. The color of the solutions of all these compounds changes from pale yellow to green−blue after the first electron has been removed. At the same time, the ferricenium absorption at $\lambda_{max} = 630$ nm appears in the UV−vis spectra. No further absorption is detected after removal of the second electron. Surprisingly, only in the case of the unsubstituted **3H−Cu** complex, the cyclic voltammogram of the dication is complementary to that of the neutral species, proving the long-term stability of [**3H−Cu**]$^{2+}$. All other derivatives **3R−Cu** tend to slowly decompose upon electron removal. After exhaustive oxidation, their cyclic voltammograms exhibit a single reversible redox process at $E^{\circ\prime} = +0.49$ V; the current flow of this single peak is almost twice as high as in the case of the two initial peaks.

Finally, we note that the first ferrocenyl oxidation in **3H−Cu** occurs at a potential value lower not only than that of **3H−M** (M = Mn, Fe, Co) complexes, but also than that of **3H−Ni** and **3H−Zn**. This means that the nature of the central atom intrinsically affects the ferrocenyl oxidation.

X-ray Crystal Structure Analyses of $(\mathbf{1H-Li})_2 \cdot 4C_6H_6$ and $\mathbf{3Cym-Cu} \cdot 2C_7H_8$. Single crystals of the lithium scorpionate **1H−Li** were obtained by slow evaporation of its benzene solution at ambient temperature. The compound crystallizes together with 4 equiv of benzene in the triclinic space group $P\bar{1}$ (Table 2; Figure 4). $(\mathbf{1H-Li})_2 \cdot 4C_6H_6$ forms centrosymmetric dimers in the solid state, in which each lithium ion binds to two tris(1-pyrazolyl)borate ligands. On the other hand, one pyrazole ring of each scorpionate fragment bridges two Li$^+$ centers, the angle Li−N(2)−Li$_a$ being 75.5(2)° (Table 3). This arrangement allows for tetracoordination of the lithium ions, even though a maximum of only three Lewis basic sites can be provided by a tripodal scorpionate ligand. It is worth mentioning that the structural motif exhibited by the $[Bpz_3]_2Li_2$ core of $(\mathbf{1H-Li})_2 \cdot 4C_6H_6$ is rather similar to the solid-state structure of the dimeric Cu(I) complex $[HBpz_3]_2Cu_2$, which also possesses two bridging pyrazolyl ligands.[16]

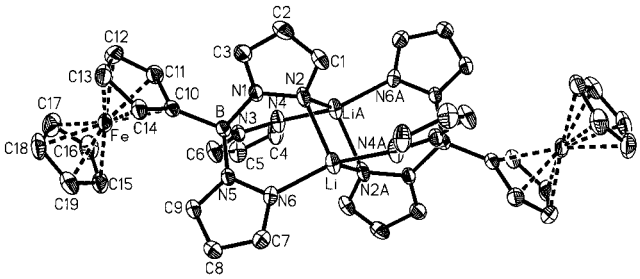

Figure 4. Molecular structure of $(\mathbf{1H-Li})_2 \cdot 4C_6H_6$; thermal ellipsoids at the 50% probability level, hydrogen atoms omitted for clarity. Symmetry transformation used to generate equivalent atoms: $-x, 1-y, -z$.

Table 3. Selected Bond Lengths (Å) and Angles (deg) of Compounds $(\mathbf{1H-Li})_2 \cdot 4C_6H_6$ and $\mathbf{3Cym-Cu} \cdot 2C_7H_8$

	$(\mathbf{1H-Li})_2 \cdot 4C_6H_6$		
B−C(10)	1.602(3)	Li−N(2)	2.081(3)
B−N(1)	1.565(3)	Li−N(6)	2.007(4)
B−N(3)	1.564(3)	Li$_a$−N(2)	2.067(4)
B−N(5)	1.554(2)	Li$_a$−N(4)	2.007(4)
N(1)−B−C(10)	105.9(1)	N(2)−Li−N(4$_a$)	102.6(2)
N(3)−B−C(10)	111.4(2)	N(2)−Li−N(6)	94.0(1)
N(5)−B−C(10)	112.1(2)	N(2$_a$)−Li−N(4$_a$)	92.9(2)
Li−N(2)−Li$_a$	75.5(2)	N(2$_a$)−Li−N(6)	113.6(2)
N(2)−Li−N(2$_a$)	104.5(2)	N(4$_a$)−Li−N(6)	144.2(2)
N(1)−B−C(10)−C(11)	80.4(2)		
	$\mathbf{3Cym-Cu} \cdot 2C_7H_8$		
B−C(10)	1.614(17)	Cu−N(2)	1.979(9)
B−N(1)	1.544(14)	Cu−N(4)	2.455(8)
B−N(3)	1.577(14)	Cu−N(6)	2.016(9)
B−N(5)	1.584(14)		
N(1)−B-C(10)	106.4(9)	N(2)−Cu−N(4)	84.0(3)
N(3)−B−C(10)	114.9(9)	N(2)−Cu−N(6)	86.9(4)
N(5)−B−C(10)	114.2(9)	N(4)−Cu−N(6)	84.1(3)
N(1)−B−C(10)−C(11)	81.7(12)		

The Li−N bond lengths involving nonbridging pyrazoles are significantly shorter (Li$_a$−N(4) = Li−N(6) = 2.007(4) Å) than the Li−N distances to the bridging pyrazole rings (Li−N(2) = 2.081(3), Li$_a$−N(2) = 2.067(4) Å). There are no short transannular contacts between either the two lithium ions or the two nitrogen centers of the central four-membered Li_2N_2 ring [Li···Li$_a$ = 2.541(6); N(2)···N(2$_a$) = 3.279(2) Å]. The ligand sphere of the lithium ions deviates considerably from an ideally tetrahedral geometry [e.g., N(2)−Li-N(6) = 94.0(1), N(2$_a$)−Li−N(4$_a$) = 92.9(2), N(4$_a$)−Li−N(6) = 144.2(2)°]. All B−N-bond lengths, as well as the bond angles around boron, fall within the normally observed ranges for structurally characterized ferrocenyltris(1-pyrazolyl)borates.[5−7] Each ferrocenyl substituent is placed into one of the three uncongested clefts made up by the pyrazole rings of its attached scorpionate moiety.

The heterotrinuclear complex $\mathbf{3Cym-Cu} \cdot 2C_7H_8$ crystallizes from toluene in the triclinic space group $P\bar{1}$ (Table 2; Figure 5).

The Cu(II) ion is located at a crystallographic inversion center and coordinated by the six nitrogen atoms of two ferrocenylscorpionate ligands. Four equatorial Cu−N bonds have average bond lengths of 2.00 Å [Cu−N(2) = 1.979(9), Cu−

(16) Mealli, C.; Arcus, C. S.; Wilkinson, J. L.; Marks, T. J.; Ibers, J. A. *J. Am. Chem. Soc.* **1976**, *98*, 711−718.

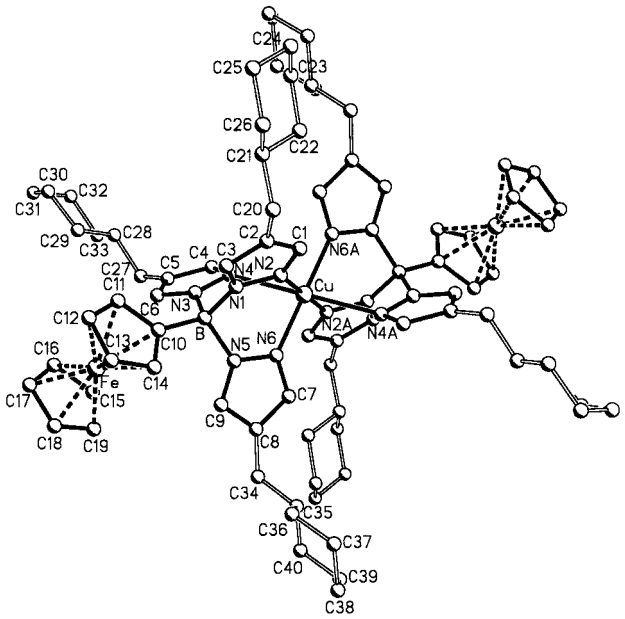

Figure 5. Molecular structure of **3Cym**−**Cu**·$2C_7H_8$; hydrogen atoms omitted for clarity.

(N6) = 2.016(9) Å], while two axial bonds are 2.46 Å long [Cu−N(4) = 2.455(8) Å]. The ligand sphere of the Cu(II) center is thus considerably affected by Jahn−Teller distortion. Interestingly, Cu−N bond elongation involves one of the two pyrazoles engulfing the Fc substituent ([N(4) to C(4)]) rather than the pyrazole ring [N(1) to C(3)], which is placed in a unique position almost perpendicular to the ferrocenyl moiety [torsion angle N(1)−B−C(10)−C(11) = 81.7(12)].

Jahn Teller distortions similar to those found in **3Cym**−**Cu**·$2C_7H_8$ have been reported for the solid-state structures of the parent complex $[HBpz_3]_2Cu$[17] and the methylated analogue $[HB(pz^{4-Me})_3]_2Cu$ (pz^{4-Me} = 4-methylpyrazolyl).[18] Both copper scorpionates, which crystallize with two independent centrosymmetric molecules in the unit cell, exhibit elongated tetragonal−octahedral CuN_6 sites with significant differences in the respective bond lengths ($[HBpz_3]_2Cu$, Cu−N bond lengths range from 2.002 to 2.530 Å in molecule A and from 1.996 to 2.357 Å in molecule B; $[HB(pz^{4-Me})_3]_2Cu$, Cu−N bond lengths range from 2.000(6) Å to 2.469(6) Å in molecule A and from 2.055(7) Å to 2.274(8) Å in molecule B). In both cases, it is apparent from a comparison of the structural data of molecules A and B, that the degree of CuN_6 distortion is greatly affected by crystal packing forces. The packing of **3Cym**−**Cu**·$2C_7H_8$ in the crystal leaves solvent-containing channels along the crystallographic *a* direction. The dimensions of these channels are slightly larger than the size required for the incorporation of toluene. The clathrated toluene molecules are therefore seriously disordered.

In summary, the geometries of dimeric (**1H**−**Li**)$_2$·$4C_6H_6$ and **3Cym**−**Cu**·$2C_7H_8$ are very similar in the solid state, as was already predicted from the IR spectroscopical results outlined above. In both molecules, significant differences are observed for the respective N−B−C(10) bond angles [(**1H**−**Li**)$_2$·$4C_6H_6$, N(1)−B−C(10) = 105.9(1), N(3)−B−C(10) = 111.4(2), N(5)−B−C(10) = 112.1(2); **3Cym**−**Cu**·$2C_7H_8$, N(1)−B−C(10) = 106.4(9), N(3)−B−C(10) = 114.9(9), N(5)−B−C(10) = 114.2(9); Table 3]. This effect is most likely due to steric repulsion between the C(6)−H [C(9)−H] group at pyrazolyl on one hand and the ferrocenyl fragment on the other.[7]

Conclusion

Ferrocene-based scorpionate ligands **1R**−**Li** and **1R**−**Tl** have been used to generate a variety of heterotrinuclear complexes **3R**−**M** (M(II) = Mn, Fe, Co, Ni, Cu, Zn). The poor solubility of the unsubstituted compounds (R = H) in all common solvents has been considerably enhanced by the introduction of large organic substituents R into the 4-position of all pyrazolyl rings [R = $SiMe_3$, cyclohexyl, (cyclohexyl)methyl, phenyl].

Compared to the parent complexes Tp_2M, the presence of ferrocenyl substituents in **3H**−**M** appears to facilitate electron removal from the coordinated metal, M [cf., Tp_2Fe: $E°'(Fe^{2+}/Fe^{3+}) = +0.32$ V; **3H**−**Fe**: $E°'(Fe^{2+}/Fe^{3+}) = +0.04$ V]. This might be due to a different bite distance of the scorpionate fragment caused by the steric effect of the bulky Fc group.[19] Cyclic voltammetric measurements also indicate a slight dependence of the Fc/Fc^+ redox potential in **3R**−**M** on the oxidation state of M (e.g., M^{2+} versus M^{3+}). While in most cases only one redox wave is observed for both ferrocenyl substituents, a striking exception was found for M = Cu. Complexes **3R**−**Cu** (R = H, Si, Cy, Cym, Ph) exhibit two well-resolved one-electron processes, corresponding to the sequential oxidation of the two Fc substituents ($\Delta E°'$ ranging from 120 to 170 mV). This observation might reflect some electronic communication between the metal centers in **3R**−**Cu**. Another possible interpretation would be that the two Fc substituents are not equal in solution on the electrochemical time scale. In this case, the Cu(II) center would have to possess a rigid ligand environment with a coordination number of five or three. This assumption, however, appears to be unlikely given the fact that the two scorpionate ligands provide six similar Lewis basic sites and that Cu(II) ions have a strong preference for either a square−planar or a symmetrical (4+2) coordination. Moreover, three-coordinated metal complexes are generally rare, and five-coordinated complexes tend to possess rather fluctional structures. The very peculiar electrochemical behavior of compounds **3R**−**Cu** is subject to further investigation.

An interesting class of heterotrinuclear complexes $[LFeMFeL]^{n+}$, which are related to **3R**−**M**, has been published by Wieghardt and collaborators [L = 1,4,7-tris(4-*tert*-butyl-2-mercaptobenzyl)-1,4,7-triazacyclononane; linear $N_3Fe(\mu\text{-}SR)_3M(\mu\text{-}SR)_3FeN_3$ core structure].[20] The degree of electron delocalization in these species is strongly dependent on the nature of the central metal, M. According to Mössbauer spectroscopy, the chromium complex $[LFeCrFeL]^{2+}$ possesses equivalent Fe centers and, therefore, has to be described as a Robin−Day class III system ($[LFe^{2.5}Cr^{III}Fe^{2.5}L]^{2+}$). The excess electron in $[LFeFeFeL]^{2+}$ is fully delocalized over all three iron sites, while the cobalt complex $[LFeCoFeL]^{2+}$ represents a temperature-dependent class II system. In contrast to previous expectations, mixed valent species were obtained even with the main group metals, M = Ge and Sn. In most cases, cyclic voltammetric measurements on $[LFeMFeL]^{n+}$ gave significantly larger dif-

(17) Murphy, A.; Hathaway, B. J.; King, T. J. *J. Chem. Soc., Dalton Trans.* **1979**, 1646−1650.
(18) Santini, C.; Pettinari, C.; Pellei, M.; Lobbia, G. G.; Pifferi, A.; Camalli, M.; Mele, A. *Polyhedron* **1999**, *18*, 2255−2259.
(19) Sohrin, Y.; Kokusen, H.; Matsui, M. *Inorg. Chem.* **1995**, *34*, 3928−3934.
(20) (a) Glaser, T.; Kesting, F.; Beissel, T.; Bill, E.; Weyhermüller, T.; Meyer-Klaucke, W.; Wieghardt, K. *Inorg. Chem.* **1999**, *38*, 722−732. (b) Glaser, T.; Bill, E.; Weyhermüller, T.; Meyer-Klaucke, W.; Wieghardt, K. *Inorg. Chem.* **1999**, *38*, 2632−2642. (c) Glaser, T.; Beissel, T.; Bill, E.; Weyhermüller, T.; Schünemann, V.; Meyer-Klaucke, W.; Trautwein, A. X.; Wieghardt, K. *J. Am. Chem. Soc.* **1999**, *121*, 2193−2208.

ferences between the Fe(II)/Fe(III) redox potentials of the two terminal iron atoms than have been observed in the case of **3R−Cu**.

Based on the results obtained for the heterotrinuclear complexes **3R−M** (e.g., relative stabilities, solubilities, electrochemical behavior), work is in progress to generate the related metal-containing polymers from difunctional ferrocene-based scorpionates **2H−Li** (Figure 1) and transition metal halides MX_2. Macromolecules with interesting electronic properties can be expected, especially in the case of M = Cu(II).

Experimental Section

All reactions and manipulations of air-sensitive compounds were carried out in dry, oxygen-free argon using standard Schlenk ware or in an argon-filled drybox. Solvents were freshly distilled under N_2 from Na/K alloy−benzophenone (toluene, hexane, THF) or from CaH_2 (CH_2Cl_2) prior to use. NMR: JEOL JMN-GX 400, Bruker DPX 400, and Bruker 250AM (abbreviations: s = singlet, d = doublet, tr = triplet, vtr = virtual triplet, q = quartet, mult = multiplet, nr = multiplet expected but not resolved, br = broad, and n.o. = not observed; Fc = $(C_5H_5)Fe(C_5H_4)$, $Hpz^{4-SiMe3}$ = 4-trimethylsilylpyrazole, Hpz^{4-Cy} = 4-cyclohexylpyrazole, Hpz^{4-Cym} = 4-(cyclohexyl)methyl-pyrazole), and Hpz^{4-Ph} = 4-phenylpyrazole). NMR spectra were recorded at ambient temperature if not stated otherwise; $h_{1/2}$ in [ ]. ^{11}B NMR shifts are given relative to external $BF_3{\cdot}Et_2O$. MS (CI, FAB mode): Finnigan MAT 90. IR: Perkin-Elmer 1650 FTIR. Elemental analyses: microanalytical laboratories of the Technische Universität München and the J. W. Goethe Universität Frankfurt.

The compounds $FcB(NMe_2)_2$, **1H−Li**, and **1H−Tl** were synthesized according to literature procedures.[5−7] All substituted complexes **1R−Tl** were prepared essentially by the procedure described below for **1Cym−Tl**.

Synthesis of $FcB(pz^{4-Cym})_3Tl$, 1Cym−Tl. A solution of 4-(cyclohexyl)methylpyrazole (2.50 g, 15.22 mmol) in 20 mL of toluene was added slowly at −78 °C to a solution of $FcBBr_2$ (1.81 g, 5.09 mmol) in 50 mL of toluene with efficient stirring. Soon afterward, neat NEt_3 (1.03 g, 10.18 mmol) was added. The mixture was allowed to warm to ambient temperature and stirred overnight. All insolubles were removed by filtration, and the filtrate was treated with a solution of TlOEt (1.25 g, 5.01 mmol) in 15 mL of toluene and stirred for 12 h. After filtration, the filtrate was evaporated to dryness under reduced pressure. The gray−brown solid residue was washed with hexane (2 × 15 mL) and dried in vacuo. Yield: 2.80 g, 63%. ^{11}B NMR (128.3 MHz, C_6D_6): δ 1.2 [170 Hz]. ^1H NMR (250.1 MHz, C_6D_6): δ 0.84 (br, 6H, C_6H_{11}), 1.07 (br, 9H, C_6H_{11}), 1.32 (br, 3H, C_6H_{11}), 1.64 (very br, 15H, C_6H_{11}), 2.27 (d, 6H, J(HH) = 6.7 Hz, CH_2), 4.19 (s, 5H, C_5H_5), 4.30, 4.41 (2 × vtr, 2 × 2H, J(HH) = 1.6 Hz, C_5H_4), 7.22 (s, 3H, pz-H3), 8.18 (s, 3H, pz-H5). ^{13}C NMR (62.9 MHz, C_6D_6): δ 26.7 (C_6H_{11}−C3,4,5), 32.7 (CH_2), 33.4 (C_6H_{11}−C2,6), 39.6 (C_6H_{11}−C1), 69.5 (C_5H_5), 70.3, 75.8 (C_5H_4), 118.1 (pz-C4), 135.1, 139.1 (pz-C3,5). ESI-MS: m/z 890 [M^+, 4.4%], 686 [$(M\text{-}Tl)^+$, 28%]. Anal. Calcd for $C_{40}H_{54}BFeN_6Tl$ (889.86): C, 53.99; H, 6.12; N, 9.44. Found: C, 53.69; H, 6.03; N, 9.69.

Synthesis of $FcB(pz^{4-Cy})_3Tl$, 1Cy−Tl. 1Cy−Tl was synthesized according to the method described for **1Cym−Tl** from 4-cyclohexylpyrazole (1.01 g, 6.72 mmol) and $FcBBr_2$ (0.80 g, 2.25 mmol). Yield: 0.61 g (32%). ^{11}B NMR (128.3 MHz, C_6D_6): δ 0.7 [130 Hz]. ^1H NMR (250.1 MHz, C_6D_6): δ 1.21 (very br, 15H, C_6H_{11}), 1.62 (br, 9H, C_6H_{11}), 1.91 (br, 6H, C_6H_{11}), 2.39 (br, 3H, C_6H_{11}), 4.24 (s, 5H, C_5H_5), 4.33, 4.44 (2 × vtr, 2 × 2H, J(HH) = 1.7 Hz, C_5H_4), 7.30 (s, 3H, pz-H3), 8.22 (s, 3H, pz-H5). ^{13}C NMR (62.9 MHz, C_6D_6): δ 26.6 (C_6H_{11}−C3,4,5), 34.5 (C_6H_{11}−C1), 35.1 (C_6H_{11}−C2,6), 69.5 (C_5H_5), 70.5, 75.6 (C_5H_4), 132.9, 136.9 (pz-C3,5), n.o. (pz-C4). Anal. Calcd for $C_{37}H_{48}BFeN_6Tl$ (847.78): C, 52.42; H, 5.71; N, 9.91. Found: C, 52.17; H, 5.62; N, 9.72.

Synthesis of $FcB(pz^{4-SiMe_3})_3Tl$, 1Si−Tl. 1Si−Tl was synthesized according to the method described for **1Cym−Tl** from 4-trimethylsilylpyrazole (0.79 g, 5.65 mmol) and $FcBBr_2$ (0.67 g, 1.88 mmol). Yield: 1.31 g (85%). ^{11}B NMR (128.3 MHz, $CDCl_3$): δ 0.6 [170 Hz]. ^1H NMR (250.1 MHz, $CDCl_3$): δ 0.11 (s, 27H, $Si(CH_3)_3$), 4.16 (s, 5H, C_5H_5), 4.24, 4.46 (2 × vtr, 2 × 2H, J(HH) = 1.5 Hz, C_5H_4), 7.45 (s, 3H, pz-H3), 8.06 (s, 3H, pz-H5). ^{13}C NMR (62.9 MHz, $CDCl_3$): δ 0.0 ($Si(CH_3)_3$), 68.9 (C_5H_5), 70.1, 75.5 (C_5H_4), 111.8 (pz-C4), 140.5, 143.7 (pz-C3,5). CI-MS: m/z 1023 [$(M + Tl)^+$, 7%], 818 [M^+, 41%]. Anal. Calcd for $C_{28}H_{42}BFeN_6Si_3Tl$ (817.97): C, 41.11; H, 5.18; N, 10.27. Found: C, 41.46; H, 5.19; N, 9.69.

Synthesis of $FcB(pz^{4-Ph})_3Li$, 1Ph−Li. To a freshly prepared solution of $FcB(NMe_2)_2$ (3.03 g, 10.67 mmol) in 60 mL of toluene, lithium 4-phenylpyrazolide (1.50 g, 9.99 mmol) in toluene (50 mL) was added at ambient temperature. After stirring for 1 h, neat 4-phenylpyrazole (2.88 g, 19.98 mmol) was added, and the mixture refluxed for 30 h. The resulting solution was evaporated to 1/5 of its original volume, cooled to 0 °C, and filtered using a filter cannula. The solid residue was triturated with hexane (10 mL) and dried in vacuo. Yield: 4.54 g (72%). ^{11}B NMR (128.3 MHz, $CDCl_3$): δ 1.6 [550 Hz]. ^1H NMR (250.1 MHz, $CDCl_3$): δ 4.03, 4.47 (2 × vtr, 2 × 2H, J(HH) = 1.6 Hz, C_5H_4), 4.33 (s, 5H, C_5H_5), 7.14−7.25 (mult, 9H, Ph-H3,4,5), 7.36 (d, 6H, Ph-H2,6), 7.49 (s, 3H, pz-H3), 8.46 (s, 3H, pz-H5). ^{13}C NMR (62.9 MHz, $CDCl_3$): δ 68.9 (C_5H_5), 69.9, 73.7 (C_5H_4), 121.8 (pz-C4), 125.2 (Ph-C2,6), 125.9 (Ph-C4), 128.7 (Ph-C3,5), 132.5 (Ph-C1), 133.8, 138.8 (pz-C3,5). Anal. Calcd for $C_{37}H_{30}BFeLiN_6$ (632.28): C, 70.29; H, 4.78; N, 13.29. Found: C, 70.00; H, 4.66; N, 13.27.

Synthesis of $FcBpz_3Mnpz_3BFc$, 3H−Mn. 1H−Li (0.59 g, 1.46 mmol) in THF (20 mL) was treated dropwise with stirring with $MnCl_2$ (0.10 g, 0.80 mmol) in H_2O (10 mL). A yellow microcrystalline solid immediately precipitated from the reaction mixture. The slurry was stirred for 0.5 h, insoluble material was collected on a frit (G3), triturated with H_2O (2 × 10 mL) and THF (10 mL), and dried in vacuo. Yield: 0.60 g (97%). ^1H NMR (400 MHz, $CDCl_3$, 303 K): δ 1.4 [80 Hz], 4.5 [330 Hz] (C_5H_5, C_5H_4). CI-MS: m/z 849 [M^+; 70%]. Anal. Calcd for $C_{38}H_{36}B_2Fe_2MnN_{12}$ (849.04) ·H_2O (18.02): C, 52.64; H, 4.42; N, 19.39; Fe, 12.9; Mn, 6.3. Found: C, 53.33; H, 4.81; N, 19.19; Fe, 12.4; Mn, 6.7.

Synthesis of $FcBpz_3Copz_3BFc$, 3H−Co. 3H−Co was synthesized in a manner similar to the synthesis of **3H−Mn**, from **1H−Li** (1.67 g, 4.13 mmol) and $CoCl_2{\cdot}6H_2O$ (0.54 g, 2.27 mmol). Yield: 1.55 g (88%). ^{11}B NMR (128.3 MHz, $CDCl_3$, 303 K): δ 240 [500 Hz]. ^1H NMR (400 MHz, $CDCl_3$, 303 K): δ −121 [1600 Hz] (pz-H3), 21.5 [60 Hz], 25.3 [30 Hz], 35 [very br], 51.0 [200 Hz] (C_5H_5, C_5H_4, pz-H4), 96 [2000 Hz] (pz-H5). CI-MS: m/z 853 [M^+; 100%]. Anal. Calcd for $C_{38}H_{36}B_2CoFe_2N_{12}$ (853.09): C, 53.51; H, 4.25; N, 19.70; Co, 6.9; Fe, 13.1. Found: C, 53.94; H, 4.35; N, 19.62; Co, 6.7; Fe, 12.6.

Synthesis of $FcBpz_3Nipz_3BFc$, 3H−Ni. Method 1. 3H−Ni was synthesized in a manner similar to the synthesis of **3H−Mn**, from **1H−Li** (1.14 g, 2.82 mmol) and $NiCl_2$ (0.19 g, 1.47 mmol). Yield: 0.93 g (77%).

Method 2. A solution of $NiBr_2{\cdot}2THF$ (0.07 g, 0.19 mmol) in THF (5 mL) was added dropwise with stirring to **1H−Tl** (0.22 g, 0.37 mmol) in THF (25 mL) at ambient temperature. The resulting orange slurry was stirred for 0.5 h, TlBr was removed by filtration, and from the filtrate, the solvent was driven off under reduced pressure. The yellow−orange residue was triturated with hexane (2 × 5 mL) and dried in vacuo. Yield: 0.15 g (95%). ^{11}B NMR (128.3 MHz, $CDCl_3$, 303 K): δ −38 [1150 Hz]. ^1H NMR (400 MHz, $CDCl_3$, 303 K): δ 4.3 [45 Hz], 4.5 [67 Hz] (C_5H_5, C_5H_4), ca. 40 [very br] (pz-H3), 46.6 [1000 Hz], 54.2 [1300] (pz-H4, pz-H5). CI-MS: m/z 852 [M^+; 100%]. Anal. Calcd for $C_{38}H_{36}B_2Fe_2N_{12}Ni$ (852.79): C, 53.52; H, 4.25; N, 19.71; Fe, 13.1; Ni. 6.9. Found: C, 53.88; H, 4.44; N, 19.41; Fe, 12.6; Ni, 7.0.

Synthesis of $FcBpz_3Znpz_3BFc$, 3H−Zn. 3H−Zn was synthesized in a manner similar to the synthesis of **3H−Mn**, from **1H−Li** (1.00 g, 2.47 mmol) and $ZnCl_2$ (0.19 g, 1.39 mmol). Yield: 0.96 g (91%). ^{11}B NMR (128.3 MHz, $CDCl_3$): δ −0.6 [260 Hz]. ^1H NMR (400 MHz, C_6D_6): δ 4.06 (s, 10H, C_5H_5), 4.26, 4.36 (2 × nr, 2 × 4H, C_5H_4), 6.01 (nr, 6H, pz-H4), 7.30 (nr, 6H, pz-H3), ca. 8.5 (very br, 6H, pz-H5). ^{13}C NMR (100.5 MHz, $CDCl_3$): δ 69.0 (C_5H_5), 70.3, 75.1 (C_5H_4), 102.8 (pz-C4), 134.2 (pz-C5), 139.2 (pz-C3). CI-MS: m/z 858 [M^+; 70%], 330 [$FcBpz_2^+$; 100%], 186 [FcH^+; 7%]. Anal. Calcd for $C_{38}H_{36}B_2Fe_2N_{12}Zn$ (859.48): C, 53.10; H, 4.22; N, 19.56; Fe, 13.0; Zn, 7.6. Found: C, 52.96; H, 4.61; N, 19.36; Fe, 12.7; Zn, 7.4.

Synthesis of $FcBpz_3Cupz_3BFc$, 3H−Cu. 3H−Cu was synthesized in a manner similar to the synthesis of **3H−Mn**, from **1H−Li** (1.00 g,

2.47 mmol) and $CuCl_2 \cdot 2H_2O$ (0.23 g, 1.35 mmol). Yield: 1.05 g (99%). ^{1}H NMR (400 MHz, $CDCl_3$, 303 K): δ 1.5 [25 Hz], 4.4 [50 Hz] (Fc). CI-MS: *m/z* 857 [M^+; 60%], 660 [(FcB(pz)(μ-pz))$_2^+$; 55%]. Anal. Calcd for $C_{38}H_{36}B_2CuFe_2N_{12}$ (857.64): C, 53.22; H, 4.23; N, 19.60; Cu, 7.4; Fe, 13.0. Found: C, 53.27; H, 4.52; N, 19.36; Cu, 7.2; Fe, 12.3. The ratio Fe:Cu of 2:1 was confirmed by TXRF measurements.

Synthesis of FcB(pz^{4-Cym})$_3$Cu(pz^{4-Cym})$_3$BFc, 3Cym−Cu. Neat $CuBr_2$ (0.04 g, 0.18 mmol) was added to a solution of **1Cym−Tl** (0.30 g, 0.34 mmol) in 40 mL of toluene with stirring at ambient temperature. The mixture, which gradually became cloudy, was stirred overnight. All insolubles were removed by filtration (filter cannula), the filtrate was evaporated under reduced pressure, and the solid residue was recrystallized from benzene/hexane (2:1) and dried in vacuo. Yield: 0.13 g (54%). X-ray quality crystals were grown by slow evaporation of a toluene solution of **3Cym−Cu** at ambient temperature. ^{1}H NMR (250.1 MHz, C_6D_6, 303 K): δ 0.4 [54 Hz], 1.1 [64 Hz], 1.5 [64 Hz], 4.3 [74 Hz] (Fc). ^{13}C NMR (62.9 MHz, $CDCl_3$, 303 K): δ 26.4, 33.6, 69.0 (Fc). ESI-MS: *m/z* 1434 [M^+, 100%]. Anal. Calcd for $C_{80}H_{108}B_2CuFe_2N_{12}$ (1434.6): C, 66.98; H, 7.58; N, 11.71. Found: C, 65.87; H, 7.54; N, 11.57. The ratio Fe:Cu of 2:1 was confirmed by TXRF measurements.

Synthesis of FcB(pz^{4-Cy})$_3$Cu(pz^{4-Cy})$_3$BFc, 3Cy−Cu. 3Cy−Cu was synthesized in a manner similar to the synthesis of **3Cym−Cu**, from $CuBr_2$ (0.04 g, 0.18 mmol) and **1Cy−Tl** (0.30 g, 0.35 mmol) in toluene. Yield: 0.10 g (42%). ^{1}H NMR (250.1 MHz, C_6D_6, 303 K): δ 0.4 [7 Hz], 1.1 [54 Hz], 1.6 [37 Hz], 1.8 [37 Hz], 4.3 [17 Hz] (Fc), 4.4 [27 Hz] (Fc). ESI-MS: *m/z* 1350 [M^+, 14%]. Anal. Calcd for $C_{74}H_{96}B_2CuFe_2N_{12}$ (1350.50): C, 65.81; H, 7.16; N, 12.44. Found: C, 65.52; H, 7.24; N, 12.03.

Synthesis of FcB(pz$^{4-SiMe_3}$)$_3$Cu(pz$^{4-SiMe_3}$)$_3$BFc, 3Si−Cu. 3Si−Cu was synthesized in a manner similar to the synthesis of **3Cym−Cu**, from $CuBr_2$ (0.04 g, 0.18 mmol) and **1Si−Tl** (0.30 g, 0.36 mmol) in toluene. The crude product was further purified by column chromatography [silica gel 60, $HCCl_3$/hexane (1:1)]. Yield: 0.10 g (43%). ^{1}H NMR (250.1 MHz, $CDCl_3$, 303 K): δ 0.5 [41 Hz] (54 H, $Si(CH_3)_3$), 1.5 [12 Hz] (12 H, pz-H3,5), 4.4 [27 Hz] (18H, Fc). ^{13}C NMR (62.9 MHz, $CDCl_3$, 303 K): δ 0.0 ($SiMe_3$), 69.2 (Fc), 69.8 (Fc). CI-MS: *m/z* 1289 [M^+, 12%]. Anal. Calcd for $C_{56}H_{84}B_2CuFe_2N_{12}Si_6$ (1290.71): C, 52.11; H, 6.56; N, 13.02: Found: C, 51.17, H, 6.94, N, 13.74. The ratio Fe:Cu of 2:1 was confirmed by TXRF measurements.

Synthesis of FcB(pz^{4-Ph})$_3$Cu(pz^{4-Ph})$_3$BFc, 3Ph−Cu. A solid mixture of **1Ph−Li** (0.63 g, 1.00 mmol) and $CuBr_2$ (0.11 g, 0.49 mmol) was dissolved in toluene/acetone (40 mL, 3:1) and stirred at ambient temperature for 3 days. The insoluble material was isolated by filtration and extracted into benzene/$HCCl_3$ (2 × 40 mL, 2:1). The extract was evaporated to dryness under reduced pressure; the remaining yellow solid triturated with acetone (10 mL) and dried in vacuo. Yield: 0.37 g (56%). ^{1}H NMR (250.1 MHz, $CDCl_3$, 303 K): δ 1.4 [3 Hz], 1.5 [1.5 Hz] (12 H, pz-H3,5), 4.5 [37 Hz] (18H, Fc), 7.1 [17 Hz] (6H, Ph-H4), 7.5 [27 Hz] (24H, Ph-H2,3,5,6). ESI-MS: *m/z* 1314 [M^+, 100%]. Anal. Calcd for $C_{74}H_{60}B_2CuFe_2N_{12}$ (1314.21): C, 67.63; H, 4.60; N, 12.79. Found: C, 67.35; H, 4.83; N, 13.06.

Reaction of 1H−Li with $CrCl_3 \cdot 6H_2O$. 1H−Li (0.62 g, 1.53 mmol) in THF (20 mL) was treated dropwise with stirring at ambient temperature with a solution of $CrCl_3 \cdot 6H_2O$ (0.22 g, 0.83 mmol) in H_2O (10 mL). The resulting brown−green slurry was stirred for 1 h, and the amount of solvent was decreased to 1/3 of the original volume under reduced pressure. Insoluble material was collected on a frit (G3), triturated with H_2O (2 × 5 mL), and dried in vacuo. Recrystallization of the crude product from CH_2Cl_2 at −30 °C afforded the boroxine **4** as dark orange needles. Yield: 0.30 g (93%). ^{11}B NMR (128.3 MHz, $CDCl_3$): δ 31.4 [320 Hz]. ^{1}H NMR (400 MHz, $CDCl_3$): δ 4.16 (s, 15H, C_5H_5), 4.53, 4.66 (2 × vtr, 2 × 6H, J(HH) = 1.8 Hz, C_5H_4). ^{13}C NMR (100.5 MHz, $CDCl_3$): δ 68.8 (C_5H_5), 73.1, 74.3 (C_5H_4). CI-MS: *m/z* 636 [M^+; 100%]. Anal. Calcd for $C_{30}H_{27}B_3Fe_3O_3$ (635.55): C, 56.70; H, 4.28. Found: C, 56.42; H, 4.57.

Crystal Structure Determination of (1H−Li)$_2 \cdot 4C_6H_6$. Suitable crystals were grown by slow evaporation of a benzene solution of **1H−Li** at ambient temperature. The compound crystallizes as a dimer together with 4 equiv of benzene. A clear yellow fragment was selected in a perfluorinated ether and mounted in a Lindemann capillary on an image plate diffraction system (IPDS; Stoe&Cie)[21] equipped with a rotating anode (ENRAF NONIUS FR591; 50 kV; 80 mA; 4.0 kW). Final lattice parameters were obtained by full-matrix least-squares refinement of 5000 reflections (graphite monochromator, $\lambda = 0.71073$ Å, Mo $K_{\bar{\alpha}}$ radiation). Data; empirical formula: $C_{38}H_{36}B_2Fe_2Li_2N_{12} \cdot 4C_6H_6$, $fw = 1120.42$, crystal size 0.29 × 0.38 × 0.44 mm, triclinic system, space group $P\bar{1}$ (I.T. No. = 2); $a = 9.8951(5)$, $b = 11.5287(6)$, $c = 13.6197(7)$ Å, $\alpha = 111.168(5)$, $\beta = 99.008(5)$, $\gamma = 100.404(5)°$, $V = 1382.8(1)$ Å^3, $Z = 1$, $\rho_{calcd} = 1.345$ g cm^{-3}. The data collection was performed at 193(1) K (Θ-range, 1.96° < Θ < 24.63°; exposure time, 900 s per image; oscillation scan mode, $\varphi = 0-360°$ with $\Delta\varphi = 1°$). A total number of 17313 reflections were collected. Raw data were corrected for Lorentz, polarization, decay, and absorption ($\mu = 0.577$ mm^{-1}) effects. After merging ($R_{int} = 0.0318$), 4384 independent reflections (all data) remained, which were used for all calculations. The structure was solved by direct methods and refined with standard difference Fourier techniques. All non-hydrogen atoms were refined anisotropically. All hydrogen atoms of the complex **1H−Li** and of one solvent molecule were found in the difference Fourier map and refined with individual isotropic thermal displacement parameters. All hydrogen atoms of the second solvent molecule were calculated in ideal positions (riding model; $U_H = 1.2\ U_C$). Additional data; number of parameters refined, 457, 9.6 data per parameter; weighting scheme, $w = 1/[\sigma^2(F_o^2)+(0.0417P)^2]$, where $P = (F_o^2+2F_c^2)/3$; shift/error < 0.001 in the last cycle of refinement; residual electron density +0.31 eÅ^{-3}, −0.23 eÅ^{-3}; $wR2 = 0.0643$ and $R1 = 0.0399$ for all data, GOF = 0.937. Neutral atom scattering factors for all atoms and anomalous dispersion corrections for the non-hydrogen atoms were taken from the International Tables for X-ray Crystallography.[22] All calculations were performed on a DEC 3000 AXP workstation and an Intel Pentium II PC with the STRUX-V system,[23] including the programs PLATON-92,[24] SIR-92,[25] and SHELXL-97.[26]

Crystal Structure Determination of 3Cym−Cu$\cdot 2C_7H_8$. Suitable crystals were grown by slow evaporation of a toluene solution of **3Cym−Cu** at ambient temperature. The compound crystallizes together with 2 equiv of toluene. A single crystal (yellow rod) was mounted on top of a glass filament on a CCD diffraction system (Bruker AXS). Final lattice parameters were obtained by full-matrix least-squares refinement of 277 reflections (graphite monochromator, $\lambda = 0.71073$ Å, Mo $K_{\bar{\alpha}}$ radiation). Data; empirical formula, $C_{80}H_{108}B_2CuFe_2N_{12} \cdot 2C_7H_8$, $fw = 1618.91$, crystal size 0.65 × 0.10 × 0.03 mm, triclinic system, space group $P\bar{1}$ (I.T. No. = 2); $a = 10.541(4)$, $b = 13.099(5)$, $c = 16.609(7)$ Å, $\alpha = 96.530(9)$, $\beta = 101.598(11)$, $\gamma = 102.849(9)°$, $V = 2159.7(15)$ Å^3, $Z = 1$, $\rho_{calcd} = 1.245$ g cm^{-3}. The data collection was performed at 136(2) K (Θ-range, 1.62° < Θ < 26.92°; exposure time, 60 s per image; scan range 610 images at $\varphi = 0$ and $\varphi = 90°$, with $\Delta\omega = 0.3°$). A total number of 10307 reflections were collected. Raw data were corrected for Lorentz, polarization, and absorption ($\mu = 0.628$ mm^{-1}) effects.[27] Transmission range for absorption: 0.891−0.981. After merging ($R_{int} = 0.1320$), 7197 independent reflections (all data) remained, which were used for all calculations. The Cu atom was placed at the origin; all other non-hydrogen atoms were taken from difference Fourier synthesis. All hydrogen atoms were calculated in ideal positions (riding model). Diffuse electron density up to 3.0 eÅ^{-3} was identified as a disordered toluene solvent molecule. Geometrical restraints were required to refine the positions of this solvent molecule.

(21) IPDS Operating System, Version 2.8.; STOE&CIE GmbH: Darmstadt, Germany, 1997.
(22) *International Tables for Crystallography*; Volume C, Tables 6.1.1.4 (pp 500−502), 4.2.6.8 (pp 219−222), and 4.2.4.2 (pp 193−199); Wilson, A. J. C., Ed.; Kluwer Academic Publishers: Dordrecht, 1992.
(23) Artus, G.; Scherer, W.; Priermeier, T.; Herdtweck, E. *STRUX-V*. A Program System to Handle X-ray Data, TU München, Germany, 1994.
(24) Spek, A. L. *Acta Crystallogr.* **1990**, A46, C34.
(25) Altomare, A.; Cascarano, G.; Giacovazzo, C.; Guagliardi, A.; Burla, M. C.; Polidori, G.; Camalli, M. *J. Appl. Crystallogr.* **1994**, *27*, 435−441.
(26) Sheldrick, G. M. *SHELXL-97*; Universität Göttingen, Germany, 1998.
(27) Sheldrick, G. M. *SADABS*. A Program for Empirical Absorption Correction of Area Detector Data; Universität Göttingen, Germany, 1996.

Additional data; number of parameters refined, 467, 15.4 data per parameter; weighting scheme, $w = 1/[\sigma^2(F_o^2)+(0.06P)^2]$, where $P = (F_o^2+2F_c^2)/3$; shift/error < 0.001 in the last cycle of refinement; residual electron density +0.88 eÅ^{-3}, −0.72 eÅ^{-3}; $wR2 = 0.2423$ and $R1 = 0.1482$ [$I > 2\sigma(I)$], GOF = 1.507. Neutral atom scattering factors for all atoms and anomalous dispersion corrections for the non-hydrogen atoms were taken from the International Tables for X-ray Crystallography.[22]

Electrochemistry. The materials and apparatus for electrochemistry have been described elsewhere.[28] All the potential values are given relative to the saturated calomel electrode (S.C.E.).

Acknowledgment. The authors wish to thank Prof. Franco Laschi for the EPR measurements on **3H−Co**. Financial funding by the "Deutsche Forschungsgemeinschaft" and the "Fonds der Chemischen Industrie" is acknowledged. P.Z. is grateful for financial support from the University of Siena (PAR 1998).

Supporting Information Available: Files in CIF format for the X-ray crystal structure determinations of (**1H−Li**)$_2$·4C_6H_6 and **3Cym−Cu**·2C_7H_8. This material is available free of charge via Internet at http://pubs.acs.org.

IC001199J

(28) Togni, A.; Hobi, M.; Rihs, G.; Rist, G.; Albinati, A.; Zanello, P.; Zech, D.; Keller, H. *Organometallics* **1994**, *13*, 1224−1234.

(29) Armstrong, W. H.; Spool, A.; Papaefthymiou, G. C.; Frankel, R. B.; Lippard, S. J. *J. Am. Chem. Soc.* **1984**, *106*, 3653−3667.